Bimetallic PdAg clusters loaded on hierarchical self-pillared pentasil zeolite as efficient catalysts for formic acid dehydrogenation

Shiyu Wan, Peng Lu, Dongyan Xu, Valentin Valtchev

Bimetallic PdAg clusters loaded on hierarchical self-pillared pentasil zeolite as efficient catalysts for formic acid dehydrogenation

Shiyu Wan [a], Peng Lu [b,*], Dongyan Xu [a,*], Valentin Valtchev [b]

[a] College of Chemical Engineering, Qingdao University of Science and Technology, Qingdao 266042, P.R. China

[b] The ZeoMat Group, Qingdao Institute of Bioenergy and Bioprocess Technology, CAS, Qingdao 266101, P.R. China.

[*]Corresponding author

E-mail: xdy0156@qust.edu.cn (D. Xu)

E-mail: lupeng@qibebt.ac.cn (P. Lu)

ABSTRACT

In the present study, siliceous self-pillared pentasil (SPP) zeolite with regular mesopores was synthesized and used as a support for anchoring bimetallic PdAg clusters through a facile impregnation-reduction method. The as-prepared PdAg/SPP catalysts with different Pd/Ag ratios were demonstrated to catalyze formic acid dehydrogenation for hydrogen production. XRD results confirmed the formation of PdAg alloy on the surface of SPP zeolite. The Pd_7Ag_3/SPP catalyst showed high activity at 80 °C with an initial turn-over frequency (TOF) of 1263.6 h^{-1}, proving the strategy using hierarchical SPP zeolite as carrier is advantageous over bulky zeolites for making highly active formic acid dehydrogenation catalysts.

Keywords: Formic acid; Hydrogen; Zeolite; Metal nanoparticles; PdAg catalysts

1. Introduction

Formic acid (FA, HCOOH) has high hydrogen-containing mass density and volume capacity of 4.4 wt% and 53.4 g/L, respectively [1]. Besides, FA can be produced from renewable feedstocks, such as biomass oxidation [2] and electrochemical reduction of carbon dioxide [3]. Those features make FA an attractive hydrogen storage material. Hydrogen can be released from FA by catalytic dehydrogenation, which has great potential as an energy carrier for fuel cells [4].

Heterogeneous catalysts are advantageous over homogeneous ones owing to their high stability and easy recyclability [5]. Although dehydrogenation over Pd-based catalysts is the dominant reaction, dehydration reaction also occurs to produce toxic CO that can poison the catalysts and deteriorate the activity and selectivity. Hence, bi- or tri-metallic alloys, such as PdAg [6,7], PdCo [8], CrAuPd [9], and AuPdPt [10], have been developed to improve the activity and selectivity. However, these metal clusters undergo sintering or aggregation during the reaction process, forming larger particles, which reduces the contact with the active site [11]. Accordingly, various types of support materials like carbon-based supports [12,13], ZrO_2 [14], *g*-C_3N_4 [15], metal-organic frameworks (MOFs) [16], etc., have been employed to disperse the nanoparticles. And those supports stabilized the nanoparticles and showed excellent catalytic activities.

Zeolites, with well-defined micropores and high stability, are excellent support candidates for confining or stabilizing metal clusters. Yu and co-workers have successfully encapsulated nanometer or sub-nanometer-sized metal clusters in MFI zeolite supports by

direct hydrothermal method, which showed excellent performance in FA dehydrogenation [17, 18]. Instead of using expensive organic precursors, Yamashita and co-workers prepared catalysts with Pd nanoparticles anchored on different zeolites (Beta, ZSM-5, and Y) using an impregnation method, and among them, with zeolite Beta-based catalyst showed the better performance toward formic acid dehydrogenation [19]. However, the sole presence of micropores in those bulky zeolite crystals could impede the encapsulation of metal precursors. The mesoporous silica material SBA-15 has been used to load bimetallic palladium-silver-based nanoparticles for catalyzing formic acid and carbon dioxide mediated-H_2 release and H_2 storage reactions [20]. Therefore, it can be expected that the Pd-based metallic NPs anchored on hierarchically porous zeolites may exhibit outstanding catalytic performance toward the selective decomposition of FA.

In this work, we synthesized a pure silica MFI zeolite, SPP (self-pillared pentasil), as the support to incorporate bimetallic PdAg clusters. The SPP zeolite is composed of two-dimensional nanosheets in an orthogonal intergrown manner, giving rise to the co-existence of micropores and mesopores. The open porous structure of SPP allowed the easy encapsulation of Pd and Ag precursors and well dispersion of metal clusters, as confirmed by HAADF-STEM mapping results. The PdAg/SPP catalyst exhibited improved activity of FA dehydrogenation.

2. Experimental

2.1. Materials and reagents

All chemicals, including tetrabutylammonium hydroxide (TBuAOH, 25%), tetraethylorthosilicate (TEOS, AR), Palladium nitrate dihydrate ($Pd(NO_3)_2 \cdot xH_2O$, Pd≥

39.0%), silver nitrate ($AgNO_3$, 99.8%), formic acid (HCOOH, 98%), sodium formate (HCOONa, 99.5%), were purchased from commercial suppliers and used as provided.

2.2. SPP zeolite synthesis

The SPP was synthesized with a reported hydrothermal method with minor modifications [21]. Typically, 49.8 g of TBuAOH solution was mixed with 33.34 g of TEOS and stirred continuously for 6 h. The obtained clear solution was transferred into a 200 mL Teflon-lined stainless steel autoclave and crystallized at 120 °C for 2 days under static conditions. The solid product was collected by centrifugation, washed with DI water until pH was close to neutral, and then dried at 80 °C in the oven. The sample was finally calcinated in the air at 550 °C for 6 h to remove the organic template.

2.3. Metal-loaded SPP catalyst preparation

SPP-supported PdAg alloy catalyst was synthesized by the wet chemical reduction method. Typically, to synthesize Pd_7Ag_3/SPP (the molar ratio of Pd to Ag is 7:3), 100 mg of SPP carrier was added to 5 mL of deionized water and stirred for 30 minutes to form a suspension. Then, added an aqueous solution containing palladium nitrate (0.1 M, 1 mL) and silver nitrate (0.1 M, 1 mL) to the suspension of SPP. After stirring for 180 minutes, add 5 mL of freshly prepared reducing agent dropwise (40 mg of sodium borohydride dissolved in 0.02 M sodium carbonate) and stir for 2 hours. The final catalyst was obtained after centrifugal separation and washing with deionized water. For comparison, Pd/SPP, Ag/SPP, and PdAg/SPP were prepared by controlling the ratio of Pd and Ag in the precursor solution (Pd_9Ag_1, Pd_7Ag_3, Pd_1Ag_1, and Pd_3Ag_7). The nominal metal loading of all catalysts is 10 wt%.

2.4. Characterizations

Powder X-ray diffraction was performed on a Rigaku SmartLab diffractometer using Cu Kα radiation at 40 kV and 150 mA. A 1D D/teX Ultra250 detector equipped with a series of linearly aligned X-ray intensity-sensing units was used to collect the diffractions in continuous scans in the theta-theta geometry at 2θ = 5-80° for phase identification. The SEM images of the powder samples were obtained using a Hitachi S-4800 Scanning Electron Microscope equipped with a cold-field emission gun operating at 5 kV. The samples were deposited on carbon tapes and inspected without coating. The transmission electronic microscopy (TEM) images were obtained from a JEOL-3200FS field-emission transmission electron microscope with an accelerating voltage of 300 kV and photographed by a Gatan OneView CMOS camera. N_2 adsorption/desorption isotherm was measured at 77 K using a Quantachrome Autosorb-iQ system. The samples were first outgassed at 300 °C for 10 h before the measurement.

2.5. Catalytic test

Typically, the catalyst (0.1 g) was first dispersed in 5 mL water and added into a two-necked round-bottomed flask placed in a water bath at a preset temperature. The reaction was initiated by introducing the aqueous solution containing 2.5 mmol FA and 2.5 mmol SF to the flask from one neck and kept magnetically stirring under 600 r/min. The volume of released gas was measured with a gas burette. The molar ratio of metal to FA (n_{metal}/n_{FA}) remains at 0.04. The initial turnover frequency (TOF) is calculated by converting 20% of FA, which is determined as the sum of the formation rates of H_2 and carbon dioxide molecules related to the theoretical number of (Pd+Ag) atoms in the

sample using the following equation:

$$TOF = \frac{PV/RT}{2n_{metal}t}$$

where P is the the atmospheric pressure, V is the volume of gas generated, R is the universal gas constant, T is the reaction temperature, n_{metal} is the molar number of metals, t is the selected reaction time.

3. Results and discussion

3.1. Characterizations of zeolite and catalysts

Fig. 1 shows the XRD patterns of the pristine SPP zeolites, the Pd/SPP, Ag/SPP, and Pd_7Ag_3/SPP catalysts. As shown in Fig. 1, the pristine SPP zeolite consistent with MFI topology (SiO_2, PDF#44-0696). The zeolite framework remained unchanged except in somewhat decreased intensity after metal deposition for all the metal-based catalysts. For Pd/SPP, the weak diffraction peaks at 39.7°, 46.2°, and 67.3° correspond to the (003), (102), and (110) planes of palladium, respectively. In the Ag/SPP sample, the characteristic peaks are located at 38.1°, 44.3°, 64.4°, and 77.4°, which correspond to the (111), (200), (220), and (311) faces of metallic Ag, respectively (PDF#87-0597). In addition to typical diffraction peaks of the MFI framework, three broad diffraction peaks were found for Pd_7Ag_3/SPP at 38.6°, 45.2°, and 65.7°, which can be attributed to the occurrence of broad diffraction peaks at 2θ between Pd (PDF#72-0710) and Ag (PDF#87-0597), clearly indicating the formation of PdAg alloys[22].

As shown in Fig. 2, all three samples in the group displayed type IV isotherms and H3 hysteresis loop, which are associated with the formation of slit-like pores by the aggregation of lamellar particles. From the pore structure parameters, as shown in Table 1,

a prominent decrease of surface area and micropore volume was observed compared to the pristine SPP after loading with PdAg nanoparticles.

As shown in Fig. 3a-b, the Pd_7Ag_3/SPP exhibits rough spherical particles, which are constructed by two-dimensional nanosheets in an orthogonal intergrown manner. The successful incorporation of Pd and Ag was further confirmed by the elemental mapping. Both Pd and Ag species are uniformly distributed on SPP.

3.2. Dehydrogenation of formic acid

The catalytic performance of the Pd_7Ag_3/SPP catalyst with reaction temperature was investigated. As shown in Fig. 4a, the reaction rate kept increasing along with elevated temperature from 25 °C to 80 °C, corresponding to an increased initial TOF from 282.2 to 1263.6 h^{-1} (Fig. 4b). It should be noted that the selectivity to H_2 is 100%, meaning that CO-free H_2 can be obtained from catalytic dehydrogenation of FA. From the Arrhenius plot ln k vs. 1/T (Fig. 4a), the activation energy of the Pd_7Ag_3/SPP catalyst was estimated to be 26.2 kJ/mol.

The catalytic performance of the PdAg/SPP catalyst with various Pd/Ag ratios, as well as the contrast Pd/SPP and Ag/SPP catalysts, were investigated at a fixed temperature of 80°C. As shown in Fig. 5a, pure SPP does not possess catalytic activity, while the Ag/SPP catalyst exhibited a low activity. In contrast, Pd/SPP exhibited much higher activity, proving that Pd plays a decisive role in formic acid dehydrogenation. When the Pd/Ag ratio increased from 3:7 to 7:3, the reaction rate can be improved gradually, but a further increasing Pd/Ag to 9:1 did not change the reaction rate anymore. Thus, the optimized Pd/Ag ratio in SPP is 7:3, from which the catalyst prepared was used for the following

studies. SF was demonstrated as an effective additive for promoting the dehydrogenation of formic acid, which could be due to the formation of electronically enriched Pd by adsorption of formate anions [23]. Thus, the effect of the FA/SF ratio on the catalytic performance of the Pd_7Ag_3/SPP catalyst was investigated (Fig. 5b). As the FA/SF ratio increased from 1:0 (pure FA) to 1:1, the reaction rate increased, and the presence of SF may increase the concentration of $HCOO^-$ ions in the solution, favoring the contact of formic acid with the active center. Although SF additive can help accelerate the dehydrogenation reaction, using pure FA would be preferable considering the cost-efficiency in practical applications. Thus, we investigated the effect of pure FA concentrations on the reaction performance (Fig. 5c). With the FA concentration increased from 0.5 M to 1.0 M, an increase in reaction rate was observed, but further increasing the concentration until 7.0 M exhibited little influence on the reaction rate.

The repeated use test of the Pd_7Ag_3/SPP catalyst for FA dehydrogenation at 80 ^oC is shown in Fig. 5d. The hydrogen production rate of the catalyst was maintained well during the three cycling tests, indicating the good stability of the Pd_7Ag_3/SPP catalyst. The slight increase in reaction time after three cycles may be due to the loss of catalyst during cycling.

4. Conclusion

Herein, pure silica SPP zeolite with MFI topology was synthesized and used as support for loading bimetallic PdAg clusters. The catalytic performance of PdAg/SPP toward hydrogen generation from FA-SF solution is highly dependent on the composition of PdAg alloy, followed by the trend of Pd_7Ag_3/SPP ≈ Pd_9Ag_1/SPP > Pd_1Ag_1/SPP >

Pd_3Ag_7/SPP. An initial TOF of 893.0 h^{-1} and H_2 selectivity of 100% can be obtained for the hydrogen generation from formic acid-sodium formate mixture aqueous solution with a FA/SF ratio of 1:1 at 80 °C over the Pd_7Ag_3/SPP catalyst. This study primarily verified the efficacy of hierarchical zeolite catalysts for FA dehydration, opening the door for more active bimetallic or multimetallic catalysts using hierarchical zeolites as support.

Declaration of Competing Interest

The authors declare no conflict of interest.

Acknowledgements

V. V. acknowledges the start-up grant provided by Qingdao Institute of Bioenergy and Bioprocess Technology (QIBEBT), and the support provided by the Shandong Energy Institute (SEI S202107). P. L. acknowledges the support by QIBEBT International Collaboration Programme (202305).

References

[1] D. Mellmann, P. Sponholz, H. Junge, M. Beller, Formic acid as a hydrogen storage material- development of homogeneous catalysts for selective hydrogen release, Chem. Soc. Rev. 45 (2016) 3954-3988.

[2] Y.J. Guo, S.J. Li, Y.L. Sun, L. Wang, W.M. Zhang, P. Zhang, Y. Lan, Y. Li, Practical DMSO-promoted selective hydrolysis-oxidation of lignocellulosic biomass to formic acid attributed to hydrogen bonds, Green Chem. 23 (2021) 7041-7052.

[3] T. Zheng, C. Liu, C. Guo, M. Zhang, X. Li, Q. Jiang, W. Xue, H. Li, A. Li, C.W. Pao, J. Xiao, C. Xia, J. Zeng, Copper-catalysed exclusive CO_2 to pure formic acid conversion via single-atom alloying, Nat. Nanotechnol. 16 (2021) 1386-1393.

[4] B. Loges, A. Boddien, H. Junge, M. Beller, Controlled generation of hydrogen from formic acid amine adducts at room temperature and application in H_2/O_2 fuel cells, Angew. Chem. Int. Edit. 47 (2008) 3962-3965.

[5] S. Zhang, B. Jiang, K. Jiang, W.B. Cai, Surfactant-free synthesis of carbon-supported palladium nanoparticles and size-dependent hydrogen production from formic acid-formate solution, ACS Appl. Mater. Interfaces. 9 (2017) 24678-24687.

[6] A. Bulut, M. Yurderi, Y. Karatas, Z. Say, H. Kivrak, M. Kaya, M. Gulcan, E. Ozensoy, M. Zahmakiran, MnOx-promoted PdAg alloy nanoparticles for the additive-free dehydrogenation of formic acid at room temperature, ACS Catal. 5 (2015) 6099-6110.

[7] X. Zhao, D. Xu, K. Liu, P. Dai, J. Gao, Remarkable enhancement of PdAg/rGO catalyst activity for formic acid dehydrogenation by facile boron-doping through $NaBH_4$ reduction, Appl. Surf. Sci. 512 (2020) 145746.

[8] C. Tang, Z. Feng, X. Bai, Magnetic N-doped partially graphitized carbon-loaded Pd-Co alloy nanoparticles for efficient hydrogen production, Colloid Surface A 648 (2022) 129348.

[9] M. Yurderi, A. Bulut, N. Caner, M. Celebi, M. Kaya, M. Zahmakiran, Amine grafted silica supported CrAuPd alloy nanoparticles: superb heterogeneous catalysts for the room temperature dehydrogenation of formic acid, Chem. Commun. 51 (2015) 11417-11420.

[10] K. Chen, Y. Liang, Z. Hu, J. Shen, Cellulose nanocrystals supported ternary alloy nanoclusters catalysts for efficient hydrogen production from formic acid, Mol. Catal. 553 (2024) 113742.

[11] J. Santos, C. Leon, G. Monnier, S. Ivanova, M. Centeno, J. Odriozola, Bimetallic PdAu catalysts for formic acid dehydrogenation, Int. J. Hydrog. Energy. 43 (2020) 23056-23068.

[12] J. Li, W. Chen, H. Zhao, X. Zheng, L. Wu, H. Pan, J. Zhu, Y. Chen, J. Lu, Size-dependent catalytic activity over carbon-supported palladium nanoparticles in dehydrogenation of formic acid, J. Catal. 352 (2017) 371-381.

[13] X. Zhang, N. Shang, H. Shang, T. Du, X. Zhou, C. Feng, S. Gao, C. Wang, Z. Wang, Nitrogen-decorated porous carbon supported AgPd nanoparticles for boosting hydrogen generation from formic acid, Energy Technol. 7 (2019) 140-145.

[14] C. Feng, S. Gao, N. Shang, X. Zhou, C. Wang, Super nanoteragonal ZrO_2 embedded

in carbon as efficient support of PdAg nanoparticle for boosting hydrogen generation from formic acid, Energy Technol. 6 (2018) 2120-2125.

[15] J. Ding, L. Wang, S.B. Stone, Y. Zhu, W. Liang, Y. Jiang, J. Huang, Nanotubular g-C_3N_4 confining AuPd particle for the improved catalytic reactivity in hydrogen production from formic acid, Mater. Today Chem. 26 (2022) 101140.

[16] Y. Ding, P. Liu, X. Huang, C. Hu, Z. Wen, Z.H. Lu, Anchoring PdAu nanoclusters inside aminated metal-organic framework for fast dehydrogenation of formic acid, Fuel 359 (2024) 130459.

[17] N. Wang, Q. Sun, R. Bai, X. Li, G. Guo, J. Yu, In situ confinement of ultrasmall Pd clusters within nanosized silicalite-1 zeolite for highly efficient catalysis of hydrogen generation, J. Am. Chem. Soc. 138 (2016) 7484-7487.

[18] Q. Sun, N. Wang, Q. Bing, R. Si, J. Liu, R. Bai, P. Zhang, M. Jia, J. Yu, Subnanometric hybrid Pd-$M(OH)_2$, M = Ni, Co, clusters in zeolites as highly efficient nanocatalysts for hydrogen generation, Chem. 3 (2017) 477-493.

[19] M. Navlani-García, M. Martis, D. Lozano-Castelló, D. Cazorla-Amorós, K. Mori, H. Yamashita, Investigation of Pd nanoparticles supported on zeolites for hydrogen production from formic acid dehydrogenation, Catal. Sci. Technol. 5 (2015) 364-371.

[20] K. Mori, S. Masuda, H. Tanaka, K. Yoshizawa, M. Che, H. Yamashita, Phenylamine-functionalized mesoporous silica supported PdAg nanoparticles: a dual heterogeneous catalyst for formic acid/CO_2-mediated chemical hydrogen delivery/storage, Chem. Commun. 53 (2017) 4677-4680.

[21] N. Wang, Q. Sun, T. Zhang, A. Mayoral, L. Li, X. Zhou, J. Xu, P. Zhang, J. Yu,

Impregnating subnanometer metallic nanocatalysts into self-pillared zeolite nanosheets, J. Am. Chem. Soc. 143 (2021) 6905-6914.

[22] F. Ke, L. Wang, J. Zhu, An efficient room temperature core-shell AgPd@MOF catalyst for hydrogen production from formic acid, Nanoscale 7 (2015) 8321-8325.

[23] P. Wang, S.N. Steinmann, G. Fu, C. Michel, P. Sautet, Key role of anionic doping for H_2 production from formic acid on Pd(111), ACS Catal. 7 (2017) 1955-1959.

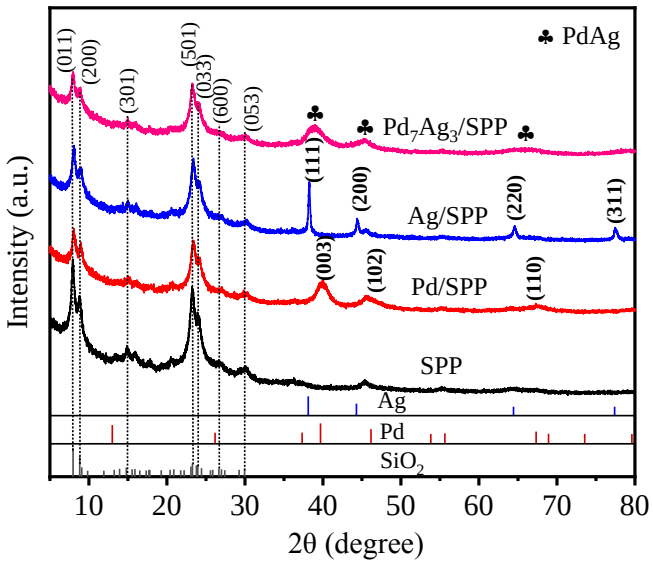

Fig. 1. XRD patterns of the pristine SPP zeolite, Pd/SPP, Ag/SPP, and Pd_7Ag_3/SPP.

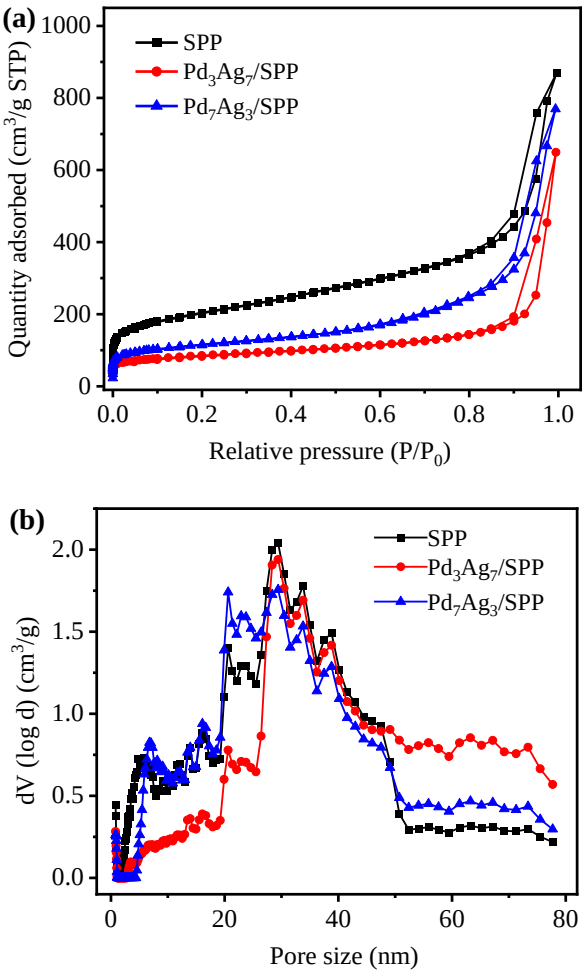

Fig. 2. (a) Nitrogen adsorption-desorption isotherms and (b) corresponding pore diameter distribution curves of the pristine SPP zeolite, Pd_3Ag_7/SPP, and Pd_7Ag_3/SPP.

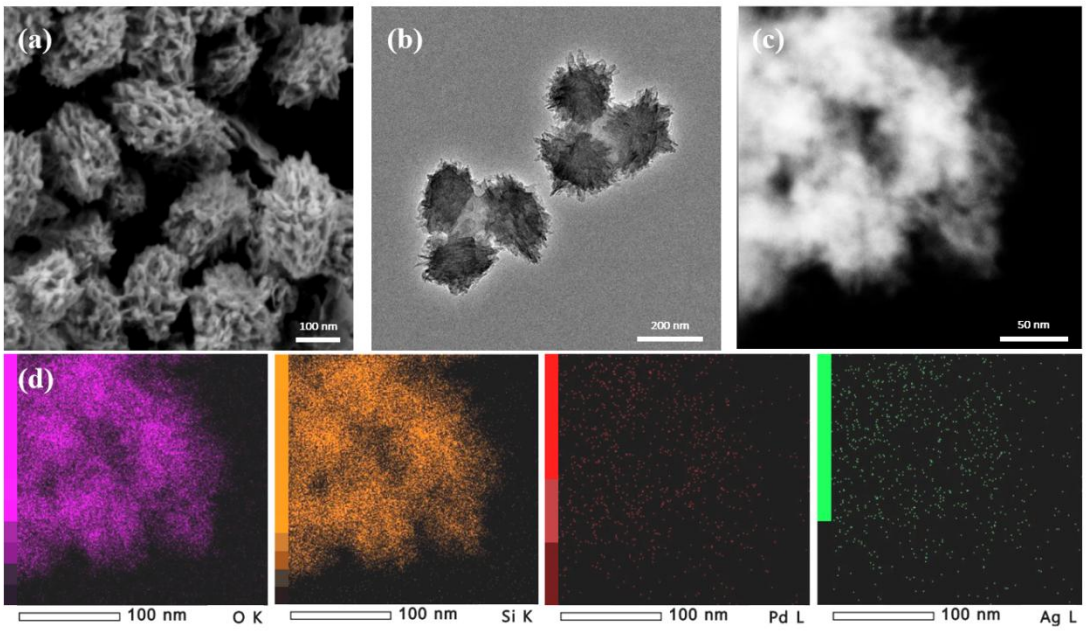

Fig. 3. SEM (a), TEM (b), HAADF-STEM image (c), and EDX elemental mappings (d) of Pd_7Ag_3/SPP.

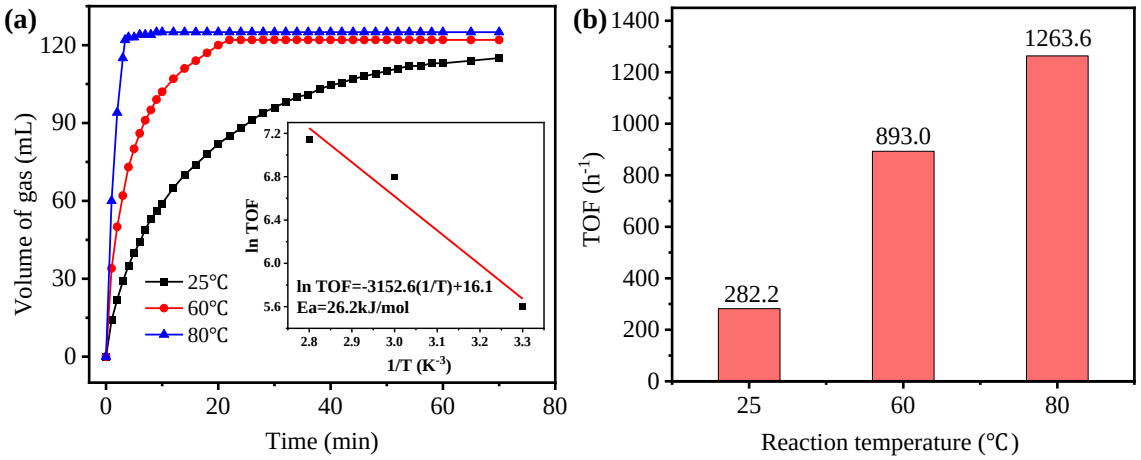

Fig. 4. Volume of generated gas (H_2 + CO_2) versus time for the dehydrogenation of FA over Pd_7Ag_3/SPP (n_{FA} = 2.5 mmol, n_{SF} = 2.5 mmol, n_{metal}/n_{FA} = 0.04) (inset: Arrhenius plot ln *k* vs. 1/T) (a) and TOF values (b) at different reaction temperatures.

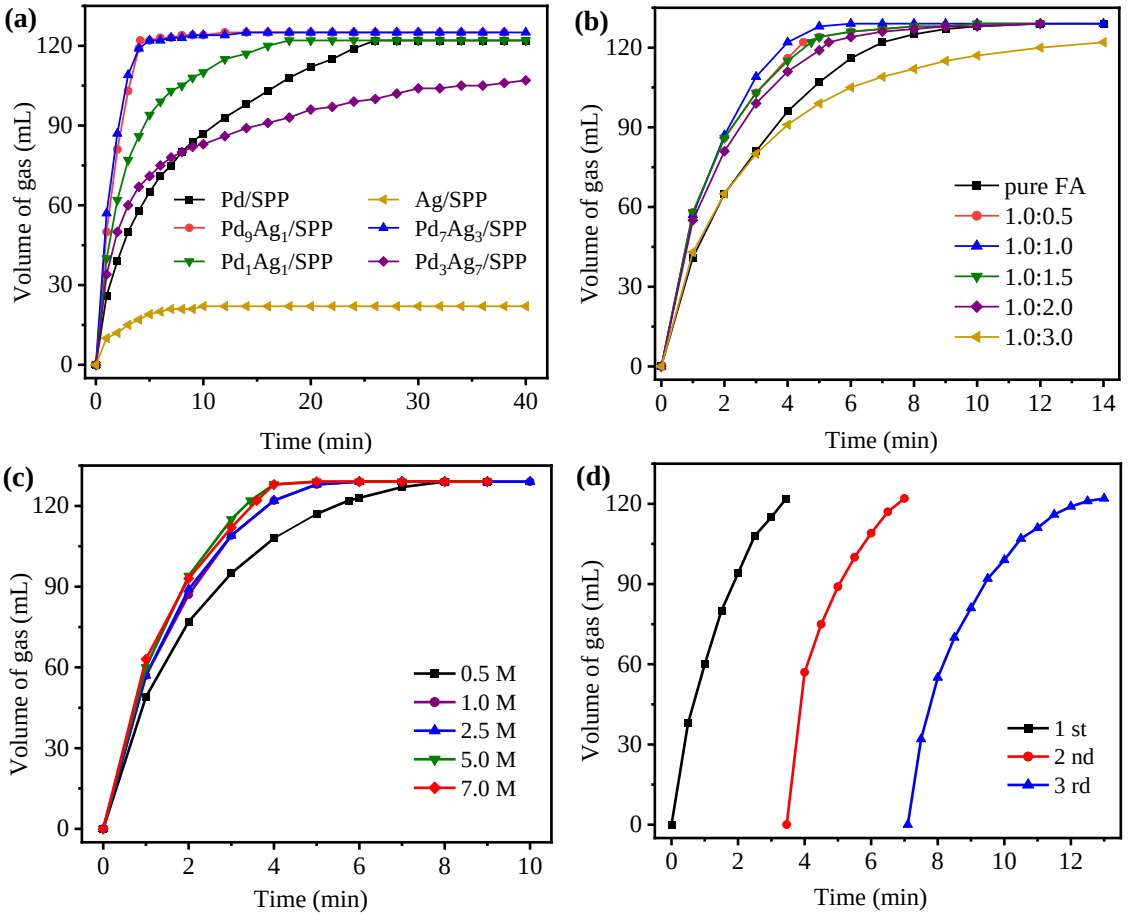

Fig. 5. Volume of generated gas (H_2 + CO_2) versus time for the dehydrogenation of FA over PdAg/SPP catalysts with different Pd to Ag molar ratios (a), under conditions of different FA to SF ratios (b), different FA concentrations (c), and cyclic test (d) over Pd_7Ag_3/SPP. (Reaction conditions: 80 ^oC, n_{FA} = 2.5 mmol, n_{SF} = 2.5 mmol, n_{metal}/n_{FA} = 0.04).